(Preprint) AAS 17-814

FAST AND RELIABLE APPROXIMATIONS FOR INTERPLANETARY LOW-THRUST TRANSFERS

Damon Landau*

A three-step process bridges the gap between lower-fidelity solutions that ignore optimal dynamics and fully optimized solutions that are computationally expensive to generate. First, analytic solutions for transfers with free time and angle characterize the evolution of the shape and orientation of the orbit. Next, optimal control theory supplies the thrust vector with variable specific impulse while satisfying flight time and transfer angle constraints. Transfers with the additional constraint of constant specific impulse then provide a more realistic thruster model for preliminary trade studies. These approximations deliver a hundredfold improvement in run time at the expense of a few percent error in mass.

INTRODUCTION

A broad view of the trajectory design space is an indispensable asset when formulating a mission concept. By gathering a complete view of the available trajectory options, lower cost and more robust designs often emerge, especially for problems where there are no existing prior point designs. While comprehensive trajectory maps are generally available for ballistic or impulsive transfers (e.g. interplanetary "pork-chop" plots or Poincaré maps), the generation of analogous maps for low-thrust transfers is a relatively tedious and time consuming process. The inherent difficulty lies in the infinite paths available to transfer from one state to another while thrusting. Approaches that have been successful for global trade space exploration include optimization, steering laws, and shape-based approaches. Each of these come with unique benefits and drawbacks: optimization produces the best solutions, but is computationally demanding with many iterations and unreliable convergence behavior; steering laws are faster with a single propagation, but are qualified as nearly optimal and typically neglect phase constraints; shape-based approaches are analytic and very fast, but generally produce infeasible thrust profiles, requiring subsequent optimization to produce reliable trajectories.

We seek a method to globally search low-thrust trajectories and inform trade studies of interplanetary missions in real time. The approach must therefore be fast (return results within the hour) and reliable (near uniform convergence with feasible and optimal thrust) to make decisions during concurrent design session whether the mission design is feasible. We consider transfers from an initial heliocentric state (3-dimensional position and velocity) and time to a final state and time, where maximum available thrust varies with the inverse square of distance from the sun. This model reflects the jet power of a solar electric propulsion system with constant specific impulse. The transfers are built in three steps of increasing accuracy and optimality as summarized in Table 1. The trajectories are modeled in a set of orbital elements

* Mission Formulation Engineer, Systems Engineering Section, Jet Propulsion Laboratory, California Institute of Technology, 4800 Oak Grove Dr., Pasadena, CA, 91109

chosen specifically for this problem, and optimized by iterating on Lagrange multipliers (i.e. the "indirect method") with special care taken to increase the region of convergence.

Table 1. A three-step process efficiently builds up to a fully optimal transfer.

Solution Phase	Initial guess for state	Initial guess for control	Accounts for phase	# of state variables	Thrust constrained	Partials wrt state
First Approximation	no	no	no	4	no	no
Suboptimal Refinement	yes	no	yes	4	no	no
Optimal Bounded Control	yes	yes	yes	7	yes	yes

APPROACH

Orbital Elements

The state of the spacecraft is specified by a set of orbital elements associated with the coordinate frame of Eq. (1), where $\{\hat{x} \quad \hat{y} \quad \hat{z}\}$ are inertial and $\hat{h}$ lies along the orbital angular momentum. This set is referred to as "axial elements" because they are designed for transfers where the angular momentum remains nearly orthogonal to an inertial axis $\hat{x}$, i.e. $\hat{g} \propto \hat{h} \times \hat{x}$. The orientation may also be specified through sequential rotations of h_Y along $\hat{x}$ then h_X along $\hat{g}$.

$$\left\{\hat{f} \quad \hat{g} \quad \hat{h}\right\} = \{\hat{x} \quad \hat{y} \quad \hat{z}\} \begin{bmatrix} \cos h_X & 0 & \sin h_X \\ \sin h_X \sin h_Y & \cos h_Y & -\cos h_X \sin h_Y \\ -\sin h_X \cos h_Y & \sin h_Y & \cos h_X \cos h_Y \end{bmatrix} \tag{1}$$

The transformation from position **r** (with magnitude *r*) and velocity **v** to the axial elements is similar to traditional equinoctial elements [1]. As implied by Eq. (1) h_X and h_Y are determined in Eq. (2) solely by the angular momentum vector. Then Eq. (3) determines the components of the eccentricity vector (in the orbital plane), and Eq. (4) specifies the true longitude along the orbit. The semi-latus rectum is a good choice for the final element, as it is valid for elliptical, parabolic, and hyperbolic orbits. However, for low-thrust transfers (often involving multiple revolutions) we are mainly concerned with elliptical orbits, and the semi-major axis ultimately results in a more succinct expression of the variational equations.

$$\begin{aligned} \hat{h} &= \left\{\hat{h}_x \quad \hat{h}_y \quad \hat{h}_z\right\}^T = \mathbf{r} \times \mathbf{v} / |\mathbf{r} \times \mathbf{v}| \\ h_X &= \sin^{-1} \hat{h}_x, \; h_Y = \tan^{-1}\left(-\hat{h}_y / \hat{h}_z\right) \end{aligned} \tag{2}$$

$$\begin{aligned} \mathbf{e} &= \left(\mathbf{v}^T \mathbf{v} / \mu - 1/r\right)\mathbf{r} - \mathbf{r}^T \mathbf{v} / \mu \, \mathbf{v} \\ e_X &= \mathbf{e}^T \hat{f}, \; e_Y = \mathbf{e}^T \hat{\mathrm{g}} \end{aligned} \tag{3}$$

$$\cos L = \mathbf{r}^T \hat{f} / r, \; \sin L = \mathbf{r}^T \hat{g} / r \tag{4}$$

$$a = 1 / \left(2/r - \mathbf{v}^T \mathbf{v} / \mu\right) \tag{5}$$

The conversion from axial elements back to position and velocity is the same as with equinoctial elements.

$$r = a\left(1-e_X^2-e_Y^2\right)\Big/\left(1+e_X\cos L+e_Y\sin L\right) \tag{6}$$

$$\begin{aligned}\mathbf{r} &= r\cos L\,\hat{f}+r\sin L\,\hat{g}\\ \mathbf{v} &= \sqrt{\mu\Big/a\left(1-e_X^2-e_Y^2\right)}\left[-\left(e_Y+\sin L\right)\hat{f}+\left(e_X\cos L\right)\hat{g}\right]\end{aligned} \tag{7}$$

The variational Eqs. (8) are also similar to those of the equinoctial elements [2] with the exception of the out-of-plane terms, which is to be expected as the axes are oriented differently. In these equations a_r, a_θ, a_h are disturbing acceleration (e.g. due to thrust) in the local radial-transverse-normal frame. Upon inspection of Eqs. (8) it becomes apparent singularities exist when $h_X = \pm\pi/2$. However, h_Y is an ignorable coordinate as is does not show up in the variational equations, thus the out-of-plane motion is completely decoupled from the in-plane dynamics when h_X is close to zero. As we shall see, it is extremely rare for the angular momentum vector to stray from the line connecting initial and final orientations along optimal interplanetary transfers. Thus the judicious choice of $\hat{x}\propto\hat{h}_0\times\hat{h}_f$ avoids these singularities because h_X optimally remains near zero. (The input position and velocity are initially rotated to an inertial frame with $\hat{x}\propto\hat{h}_0\times\hat{h}_f$ then rotated back for output.) We thus trade the coupled equinoctial equations with a single singularity (when the orbit goes completely retrograde), for axial elements that remain decoupled and circumvent the singular axis as the orbit optimally transfers from initial to final orientation.

$$\begin{aligned}da/dt &= \frac{2a^2}{h}\left[\left(e_X\sin L-e_Y\cos L\right)a_r+\left(1+e_X\cos L+e_Y\sin L\right)a_\theta\right]\\ de_X/dt &= \frac{h}{\mu}\sin L\;a_r+\left[\frac{h}{\mu}\cos L+\frac{r}{h}\left(e_X+\cos L\right)\right]a_\theta+e_Y\frac{r}{h}\tan h_X\cos L\;a_h\\ de_Y/dt &= -\frac{h}{\mu}\cos L\;a_r+\left[\frac{h}{\mu}\sin L+\frac{r}{h}\left(e_Y+\sin L\right)\right]a_\theta-e_X\frac{r}{h}\tan h_X\cos L\;a_h\\ dh_X/dt &= \frac{r\sin L}{h}a_h\\ dh_Y/dt &= \frac{r\cos L}{h\cos h_X}a_h\\ dL/dt &= \frac{h}{r^2}-\frac{r}{h}\tan h_X\cos L\;a_h\end{aligned} \tag{8}$$

where

$$h^2 = \mu\left(1+e_X\cos L+e_Y\sin L\right)/r = \mu a\left(1-e_X^2-e_Y^2\right) \tag{9}$$

Because the dynamics are sensitive to the fast variable L and do not depend on time, it is advantageous to switch the independent variable from time to true longitude. The acceleration **a** due to solar electric propulsion varies as $1/r^2$, leading to a natural choice of control **u** in the form of Eq. (10). These two modifications to the variational equations cancel the r^2 terms in Eq. (11). With the assertion that $h_x \neq 1$ the variational equations with respect to L then become Eqs. (12). In this set of elements, h_X, h_Y, and t become ignorable coordinates and only dt/dL depends on $\alpha = \ln a$.

$$\mathbf{u} = \left\{u_r \quad u_\theta \quad u_h\right\}^T = \mathbf{a}\Big/\left(\mu/r^2\right) \tag{10}$$

$$\mathbf{a}dt = \mathbf{u}\frac{\mu}{r^2}\frac{r^2}{h}dL = \frac{\mu}{h}\mathbf{u}dL \tag{11}$$

$$\begin{aligned}
d\alpha/dL &= \frac{2}{\left(1-e_X^2-e_Y^2\right)}\left[\left(e_X\sin L - e_Y\cos L\right)u_r + \left(1+e_X\cos L + e_Y\sin L\right)u_\theta\right] \\
de_X/dL &= \sin L\, u_r + \left(\cos L + \frac{e_X+\cos L}{1+e_X\cos L+e_Y\sin L}\right)u_\theta \\
de_Y/dL &= -\cos L\, u_r + \left(\sin L + \frac{e_Y+\sin L}{1+e_X\cos L+e_Y\sin L}\right)u_\theta \\
dh_X/dL &= \frac{\sin L}{1+e_X\cos L+e_Y\sin L}u_h \\
dh_Y/dL &= \frac{\cos L}{\left(1+e_X\cos L+e_Y\sin L\right)}u_h \\
dt/dL &= \sqrt{\exp(3\alpha)\left(1-e_X^2-e_Y^2\right)^3/\mu}\Big/\left(1+e_X\cos L+e_Y\sin L\right)^2
\end{aligned} \tag{12}$$

First Approximation

An initial guess for how the "slow" elements (α, e_X, e_Y, h_X, h_Y) vary with respect to each other is determined by initially ignoring phase angle and time. We begin by solving for the optimal thrust program to minimize the square of the control magnitude over a single orbit, Eq. (13). The motion of the eccentricity vector is tracked in orbital plane coordinates for each orbit, where Eq. (15) maps the change in axial coordinates to orbital plane coordinates. We account for the equations of motion while minimizing ΔJ by adjoining Eq. (16) to the objective via Lagrange multipliers in Eq. (17). For time-free transfers the control can be vanishingly small and the Lagrange multipliers remain constant [1]. The partial of ΔJ^* with respect to the controls **u** provides the optimal control profile, Eq. (18). Then, the choice of how the elements change per orbit determines the Lagrange multipliers in Eq. (19) by substituting Eq. (18) into Eq. (16), and governs the cost of Eq. (21).

$$\Delta J = 1/2\int_0^{\Delta t}\mathbf{u}^T\mathbf{u}dt = 1/2\int_0^{2\pi}\mathbf{u}^T\mathbf{u}\left(dt/dL\right)dL \tag{13}$$

$$\Delta t = 2\pi\sqrt{a^3/\mu} \tag{14}$$

$$\begin{Bmatrix}\Delta e_e \\ \Delta e_p\end{Bmatrix} = \frac{1}{e}\begin{bmatrix} e_X & e_Y \\ -e_Y & e_X\end{bmatrix}\begin{Bmatrix}\Delta e_X \\ \Delta e_Y\end{Bmatrix} \tag{15}$$

$$\begin{aligned}
\Delta\mathbf{X} &= \begin{Bmatrix}\Delta\alpha & \Delta e_e & \Delta e_p & \Delta h_X & \Delta h_Y\end{Bmatrix}^T = \int_0^{2\pi}\mathbf{f}_\mathbf{u}\mathbf{u}dL \\
\mathbf{f} &= d\begin{Bmatrix}\alpha & e_e & e_p & h_X & h_Y\end{Bmatrix}^T/dL
\end{aligned} \tag{16}$$

$$\Delta J^* = \Delta J + \int_0^{2\pi}\boldsymbol{\lambda}^T\left(\Delta\mathbf{X} - \mathbf{f}_\mathbf{u}\mathbf{u}\right)dL \tag{17}$$

$$\Delta J_\mathbf{u}^* = \mathbf{u}\,dt/dL - \mathbf{f}_\mathbf{u}^T\boldsymbol{\lambda} = 0 \rightarrow \mathbf{u} = \mathbf{f}_\mathbf{u}^T\boldsymbol{\lambda}/\left(dt/dL\right) \tag{18}$$

$$\Delta\mathbf{X} = \mathbf{F}\boldsymbol{\lambda} \rightarrow \boldsymbol{\lambda} = \mathbf{F}^{-1}\Delta\mathbf{X} \tag{19}$$

$$\mathbf{F} = \int_0^{2\pi} \frac{\mathbf{f_u}\mathbf{f_u}^T}{dt/dL}\,dL = \pi\sqrt{\frac{\mu/a^3}{\left(1-e^2\right)^3}}\begin{bmatrix} \frac{4\left(2+7e^2+e^4\right)}{\left(1-e^2\right)^2} & 4e\left(4+e^2\right)/\left(1-e^2\right) & 0 & 0 & 0 \\ 4e\left(4+e^2\right)/\left(1-e^2\right) & 5+5e^2 & 0 & 0 & 0 \\ 0 & 0 & 5+e^2 & 0 & 0 \\ 0 & 0 & 0 & 1 & 0 \\ 0 & 0 & 0 & 0 & 1 \end{bmatrix} \tag{20}$$

$$\Delta J = 1/2\,\Delta\mathbf{X}^T\mathbf{F}^{-1}\left(\int_0^{2\pi}\mathbf{f_u}\mathbf{f_u}^T/\left(dt/dL\right)dL\right)^{-1}\mathbf{F}\Delta\mathbf{X} = 1/2\,\Delta\mathbf{X}^T\mathbf{F}^{-1}\Delta\mathbf{X} \tag{21}$$

Equation (20) is the solar electric analogue of the constant thrust approximation developed by Edelbaum [3]. Unlike the constant thrust case changes the semi-major axis and eccentricity are coupled, which significantly complicate the calculation of $\mathbf{F}^{-1}$. We circumvent this nuisance by nullifying the off-diagonal terms in $\mathbf{F}$ and approximating the cost of an uncoupled system. (This approximation remains accurate for moderate eccentricities.) The choice of quadratic cost in Eq. (13) simplifies the optimization over a single orbit, but a minimization of the magnitude of the control, Eq. (22), is ultimately desired for typical low-thrust transfers. The Cauchy-Schwarz inequality Eq. (23) provides an approximation of the minimum magnitude of this cost in Eq. (24). Thus far the analysis has considered the cost over a single orbit, but minimization of the total cost along the path from initial state to final state determines the optimal variation of elements. Equation (25) determines the incremental cost dU for an infinitesimal change in elements along the path ds by substituting Eqs. (21) and Eq. (14) into Eq. (24) (with the assumption that the path comprises many revolutions). Motion of h_X is not considered in Eq. (25) because it begins and ends at zero and any excursion from zero would unnecessarily increase the cost. We now seek a solution to how all the other elements optimally change given a variation in any single element.

$$\Delta U = \int_0^{\Delta t}\sqrt{\mathbf{u}^T\mathbf{u}}dt \tag{22}$$

$$\left(\int_0^{\Delta t}\sqrt{\mathbf{u}^T\mathbf{u}}dt\right)^2 \le \Delta t\int_0^{\Delta t}\mathbf{u}^T\mathbf{u}dt \tag{23}$$

$$\Delta U \approx \sqrt{2\Delta t\Delta J} \tag{24}$$

$$\frac{dU}{ds} = \dot{U} = \sqrt{\frac{a^3 2\left(1-e^2\right)^{3/2}}{\mu}\left[\frac{\left(1-e^2\right)^2\dot{\alpha}^2}{4\left(2+7e^2+e^4\right)} + \frac{\dot{e}_e^2}{5+5e^2} + \frac{\dot{e}_p^2}{5+e^2} + \dot{h}_Y^2\right]} \tag{25}$$

Following Edelbaum [4], the cost of changing the eccentricity and orientation determines the optimal change in semi-major axis by noting that e_e, e_p, and h_Y depend on a to the same power. Thus the path of Eq. (27) controls the optimal path of a in the following manner. If we neglect the potential coupling of w_a and ψ (i.e. $\partial\dot{U}/\partial\psi = 0$), then applying the Euler-Lagrange equation to $\dot{\psi}$ provides a constant of integration in Eq. (28). Equation (30) gives ψ^* as a function of a after integrating Eq. (29). The boundary conditions that a begins at a_0 and ends at a_f solve for the constant k, and inverting Eq. (30) produces Eq. (32) of how a (approximately) optimally varies as a function of ψ^*. Once the sub-cost ψ^* is determined, Eq. (33) can be used to determine the total cost.

$$\dot{U} = \sqrt{a^3\left(w_a\,\dot{a}^2/a^2 + \dot{\psi}^2\right)},\ w_a = 2\left(1-e^2\right)^{7/2}\Big/\left[\mu 4\left(2+7e^2+e^4\right)\right] \tag{26}$$

$$\dot{\psi}^2 = \frac{2}{\mu}\left(1-e^2\right)^{3/2}\left(\frac{\dot{e}_e^2}{5+5e^2} + \frac{\dot{e}_p^2}{5+e^2} + \dot{h}_y^2\right) \tag{27}$$

$$\frac{d}{ds}\left[\sqrt{a^3\dot{\psi}^2\Big/\left(w_a\,\dot{a}^2/a^2+\dot{\psi}^2\right)}\right] = 0 \rightarrow a^3\dot{\psi}^2\Big/\left(w_a\,\dot{a}^2/a^2+\dot{\psi}^2\right) = 1/k \tag{28}$$

$$\dot{\psi}\Big/\sqrt{w_a} = \dot{a}\Big/\left(a\sqrt{ka^3-1}\right) \tag{29}$$

$$\psi^*(s) = 1.5\int \dot{\psi}\Big/\sqrt{w_a}\,ds = \tan^{-1}\sqrt{ka^3-1} \tag{30}$$

$$k = -\tan^{-1}\left[\sin\psi_f^*\Big/\left(\cos\psi_f^* - a_0^3/a_f^3\right)\right] \tag{31}$$

$$a(s) = a_0\left[\sin k\Big/\sin\left(\psi^*(s)+k\right)\right]^{2/3} \tag{32}$$

$$\dot{\alpha} = -\dot{\psi}\Big/\left[\sqrt{w_a}\tan\left(\psi^*+k\right)\right] \tag{33}$$

Now, the problem remains of determining $\dot{\psi}$ along the transfer. In Eq. (34) it is noted that h_Y is an ignorable coordinate, and the Euler-Lagrange equation again provides a constant of integration in Eq. (35). The solution to Eq. (36) governs the optimal change in h_Y as a function of the eccentricity vector. Unfortunately this functional form can lead to nearly impulsive maneuvers when the change in orbit plane is much larger than the change in eccentricity, which is somewhat expected the integral of a magnitude, Eq. (22). Instead the nearly optimal approximation of Eq. (37) is used to determine how h_Y should vary with eccentricity for low-thrust transfers. The last step is to determine how e_X and e_Y should vary along the transfer path. Reference [4] provides solutions to two simplified problems, but offers no general solution. It is observed, however, that the eccentricity vector usually does not stray far from a straight line connecting the initial and final points for very low thrust transfers. We therefore make a heuristic argument to solve for the optimal variation in orbital elements by beginning with a straight path through eccentricity space, Eq. (38). (Again, $\dot{e}_X, \dot{e}_Y$ maps to $\dot{e}_e, \dot{e}_p$ via Eq. (15).)

$$\dot{\psi}^2 = \dot{\varepsilon}^2 + w_h\dot{h}_Y^2,\ \dot{\varepsilon}^2\left(e_e, e_p\right) = w_h\left(\frac{\dot{e}_e^2}{5+5e^2} + \frac{\dot{e}_p^2}{5+e^2}\right),\ w_h = \frac{2}{\mu}\left(1-e^2\right)^{3/2} \tag{34}$$

$$\frac{d}{ds}\left[\sqrt{w_h\dot{h}_Y^2\Big/\left(\dot{\varepsilon}^2 + w_h\dot{h}_Y^2\right)}\right] = 0 \rightarrow w_h^2\dot{h}_Y^2\Big/\left(\dot{\varepsilon}^2 + w_h\dot{h}_Y^2\right) = \kappa \tag{35}$$

$$\dot{h}_y = \sqrt{\dot{\varepsilon}^2\Big/\left[w_h\left(w_h/\kappa - 1\right)\right]} \tag{36}$$

$$\dot{h}_Y \propto \sqrt{\dot{\varepsilon}^2/w_h},\ \dot{h}_Y = h_{Y,f}\sqrt{\dot{\varepsilon}^2/w_h}\Big/\left(\int_0^1\sqrt{\dot{\varepsilon}^2/w_h}\,ds\right) \tag{37}$$

$$\begin{aligned} &\dot{e}_X = e_{X,f} - e_{X,0},\ \dot{e}_Y = e_{Y,f} - e_{Y,0} \\ &e_X(s) = e_{X,0} + \dot{e}_X s,\ e_Y(s) = e_{Y,0} + \dot{e}_Y s,\ s = [0,1] \end{aligned} \tag{38}$$

A first approximation to optimal time-free transfers from initial to final axial elements with inverse square power begins by specifying the path through eccentricity space Eq. (38), then solving for the evolution of the orbital plane, Eq. (37), and finally determining how the semi-major axis changes as a function of these elements via Eq. (32). The resulting cost provides an approximation of the transfer ΔV in Eq. (39), where the average of $1/r^2$ over an orbit is used in Eq. (40).

$$\Delta \mathrm{V} = \int \sqrt{\mathbf{a}^T \mathbf{a}} dt = \int \sqrt{\mathbf{u}^T \mathbf{u}}\, \mu / r^2\, dt \approx \int_0^1 \mu \dot{U} \Big/ \left(a^2 \sqrt{1-e^2} \right) ds \tag{39}$$

$$\overline{r^{-2}} = \frac{1}{\Delta t} \int_0^{\Delta t} r^{-2} dt = \frac{1}{\Delta t} \int_0^{2\pi} \left[\mu a \left(1-e^2\right) \right]^{-1/2} d\nu = \frac{1}{a^2 \sqrt{1-e^2}} \tag{40}$$

We complete the state description for the initial guess by specifying how the true longitude *L* should vary along the transfer. The integral of the mean motion weighted by the incremental cost along the path approximates the mean anomaly in Eq. (41). The number of revolutions *N* is a free design parameter, and the mean anomaly provides a good estimate in Eq. (42) where the final longitude is adjusted by $2\pi N$ in Eq. (43). The optimal value is typically within ± one revolution of this estimate. In Eq. (44) the mean anomaly estimate is made to match the true longitude bounds (as we still haven't considered variations within a single orbit) and completes a full state description of the transfer as a function of the path variable *s*.

Before further numerical optimization, we seek to model the path as a series of *n* segments. The somewhat arbitrary choice of constant change in eccentricity vector does not necessarily lend itself to a useful discretization of the path (e.g. many orbits could clump where the other elements change quickly relative to eccentricity). It is found that breaking the change in true longitude into segments inversely proportional to the orbit period as in Eq. (45) (so there are more segments on bigger orbits) improves subsequent convergence. The true longitude at segment boundaries L_B is distributed evenly with respect to *s* as in Eq. (47), and the states are defined at the segment midpoints in Eq. (47). The path is essentially redistributed by shifting *ds* so that *M* aligns with *L*. This series of segments can be thought of as an updated path variable where each segment represents and unitary change in *s* from 0 to *n*.

$$M^* = \frac{TOF}{U_f} \int \sqrt{\mu / a^3}\, \dot{U} ds \tag{41}$$

$$N = \left\| \left(M_f^* - \Delta \right) / 2\pi \right\| \vee 0,\ \Delta = \left(L_f - L_0 \right) \bmod 2\pi \tag{42}$$

$$L_f = L_0 + \Delta + 2\pi N \tag{43}$$

$$M(s) = L_0 + \left(L_f - L_0 \right) M^* / M_f^* \tag{44}$$

$$\begin{aligned} &dL \propto a^{-3/2} ds \rightarrow w_L = \int a^{-3/2} ds \\ &L(s) = L_0 + \left(L_f - L_0 \right) w_L / w_{L,f} \end{aligned} \tag{45}$$

$$L_{B,i} = L\left(s = i/n \right),\ i = 0, \ldots, n \tag{46}$$

$$L_i = \left(L_{B,\mathrm{i}-1} + L_{B,\mathrm{i}}\right)\big/2,\ \mathbf{X}\left(L_i\right) = \mathbf{X}\left(s\big|_{M=L_i}\right),\ i = 1,\ldots,n \tag{47}$$

There is certainly opportunity to reduce the cost (or ΔV) of this initial guess by choosing a different eccentricity path or including coupling of eccentricity and semi-major axis at the expense of a more complex algorithm. We forego complicating the algorithm further as this solution is only a first approximation of the low-thrust transfer, and more sophisticated approximations will come to bear in subsequent analyses.

Suboptimal Refinement

The next step is to include variations of the trajectory within each orbit and account for phasing and transfer time. Typically this would require numerical integration of the equations of motion. However, if we break the transfer into a moderate number of segments (say 10–20 per revolution) and assume that the semi-major axis and eccentricity remain constant and the thrust direction is fixed over each segment then the variation of the orbital elements over each segment can be determined analytically. In this way the trajectory calculation only requires a modest number of segments to capture the underlying dynamics, ultimately requiring fewer computations than numerical integration [5],[6]. After integrating Eqs. (12) over a segment Δs, the corresponding set of variational equations for axial elements are calculated via Eqs. (48). The segment boundaries are defined in Eq. (49) and occur at the midpoint between the nodes where the state is defined in Eq. (47). The values for L at the segment nodes and boundaries remain fixed.

The derivation of the integrals in Eqs. (52) and (53) were greatly simplified by first rotating to orbital plane coordinates via Eq. (50). It should be noted that $\Delta\nu = \Delta L$ because the axial elements are constant on each segment. The true longitude is continuous throughout, but the true anomaly is discontinuous across segment boundaries. It appears that the variational equations become singular when $e = 0$, but this is merely an artifact of expressing the integrals in orbital plane coordinates. Equations (54) are suitable if the eccentricity becomes vanishingly small.

$$\begin{aligned}
\Delta\alpha/\Delta s = \dot{\alpha} &= -\frac{2\left(\mathrm{e}\cos\nu^{+} - e\cos\nu^{-}\right)}{\left(1-e^2\right)}u_r + \frac{2\left(\Delta\nu + \mathrm{e}\sin\nu^{+} - e\sin\nu^{-}\right)}{\left(1-e^2\right)}u_\theta \\
\dot{e}_x &= -\Delta\cos L\ u_r + \left(\ \Delta\sin L + \frac{e_X}{e^2}I_1 - \frac{e_Y}{e^2}I_2\right)u_\theta \\
\dot{e}_y &= -\Delta\sin L\ u_r + \left(-\Delta\cos L + \frac{e_X}{e^2}I_2 + \frac{e_Y}{e^2}I_1\right)u_\theta \\
\dot{h}_x &= \left(\frac{e_X}{e^2}I_2 - \frac{e_Y}{e^2}I_3\right)u_h \\
\dot{h}_y &= \left(\frac{e_X}{e^2}I_3 + \frac{e_Y}{e^2}I_2\right)u_h \\
\dot{t} &= \sqrt{\frac{a^3\left(1-e^2\right)}{\mu}}\left[\Delta\chi - \left(1-e^2\right)\left(\frac{e\sin\nu^{+}}{1+e\cos\nu^{+}} - \frac{e\sin\nu^{-}}{1+e\cos\nu^{-}}\right)\right]
\end{aligned} \tag{48}$$

where

$$L^{-} = L_{B,i-1},\ L^{+} = L_{B,i} \tag{49}$$

$$\begin{Bmatrix} e\cos\nu \\ e\sin\nu \end{Bmatrix} = \begin{bmatrix} e_X & e_Y \\ -e_Y & e_X \end{bmatrix} \begin{Bmatrix} \cos L \\ \sin L \end{Bmatrix},\ e^2 = e_X^2 + e_Y^2 \tag{50}$$

$$\Delta\cos L = \cos L^+ - \cos L^-,\ \Delta\sin L = \sin L^+ - \sin L^-,\ \Delta\nu = \Delta L = L^+ - L^- \tag{51}$$

$$\Delta\chi = 2\sqrt{1-e^2}\,\tan^{-1}\left(\sqrt{1-e^2}\Big/\left[\left(1+e\cos\nu^-\right)\frac{\cos L^+ + \cos L^-}{\sin L^+ - \sin L^-} - e\sin\nu^-\right]\right) \tag{52}$$

$$I_1 = \Delta\nu - \Delta\chi,\ I_2 = \log\left(1 - e\frac{\cos\nu^+ - \cos\nu^-}{1+e\cos\nu^+}\right),\ I_3 = \frac{\Delta\chi}{\left(1-e^2\right)} - \Delta\nu \tag{53}$$

$$\begin{aligned} \dot{e}_X\big|_{e=0} &= -\Delta\cos L\ u_r + 2\Delta\sin L\ u_\theta,\ \dot{e}_Y\big|_{e=0} = -\Delta\sin L\ u_r - 2\Delta\cos L\ u_\theta \\ \dot{h}_X\big|_{e=0} &= -\Delta\cos L\ u_h,\ \dot{h}_Y\big|_{e=0} = \ \Delta\sin L\ u_h \end{aligned} \tag{54}$$

The propulsion system model for this step is power limited, but the specific impulse (and thrust) can optimally vary as reflected in Eqs. (55)–(57), where P_1 is the jet power at 1 AU. The objective Eq. (58) is to maximize the final mass or equivalently minimize the square of the control effort. As with the prior analysis of Eq. (13), this problem is easier to solve than the constant specific impulse model because the thrust magnitude is not constrained. We first optimize only the in-plane motion Eqs. (59) then solve the out-of-plane dynamics afterwards, taking advantage that the angular momentum does not affect the dynamics in Eq. (48) and the cost associated with u_h is separable from the in-plane term of J.

$$dm/dt = -m^2\mathbf{a}^T\mathbf{a}\Big/\left[2P_1\left(AU/r\right)^2\right] \tag{55}$$

$$dm/dL = -m^2\mu^2\mathbf{u}^T\mathbf{u}\Big/\left[2P_1AU^2\sqrt{\mu a\left(1-e_X^2-e_Y^2\right)}\right] \tag{56}$$

$$\dot{m} = m^2 w_m\mathbf{u}^T\mathbf{u}/2,\ w_m = -\Delta L\mu^{3/2}\Big/\left[P_1AU^2\sqrt{a\left(1-e_X^2-e_Y^2\right)}\right] \tag{57}$$

$$J = 1/m_f - 1/m_0 = 1/2\int w_m\left(u_r^2 + u_\theta^2\right)ds + 1/2\int w_m u_h^2 ds \tag{58}$$

$$\begin{aligned} &\mathbf{X} = \begin{Bmatrix} \alpha & e_X & e_Y & t \end{Bmatrix}^T,\ \mathbf{f} = \dot{\mathbf{X}} \\ &\boldsymbol{\lambda} = \begin{Bmatrix} \lambda_\alpha & \lambda_{e_X} & \lambda_{e_Y} & \lambda_t \end{Bmatrix}^T,\ \boldsymbol{\upsilon} = \begin{Bmatrix} u_r & u_\theta \end{Bmatrix}^T \end{aligned} \tag{59}$$

The Hamiltonian Eq. (60) of this optimization problem determines the dynamics of the Lagrange mulitpliers $\boldsymbol{\lambda}$ via Eq. (61) [7]. We further simplify the dynamics by (suboptimally) decoupling the propagation of the Lagrange multipliers from the controls by assuming that $\boldsymbol{\upsilon} = \mathbf{0}$ at the beginning of each iteration. As demonstrated in Eq. (62), only $\dot{t}$ has non-zero partials that affect the propagation of $\dot{\boldsymbol{\lambda}}$, resulting in the relatively simple solution of Eq. (63). This model is computationally efficient because the partials of the other elements are not required. The optimal value of $\boldsymbol{\upsilon}$ makes the partial of the Hamiltonian vanish [7] and solves for the control as a function of final values of $\boldsymbol{\lambda}$ in Eq. (64).

$$H = \vartheta + \boldsymbol{\lambda}^T\mathbf{f} + 1/2\,w_m u_h^2 + \lambda_{h_X}\dot{h}_X + \lambda_{h_Y}\dot{h}_Y,\ \vartheta = 1/2\,w_m\boldsymbol{\upsilon}^T\boldsymbol{\upsilon} \tag{60}$$

$$H_{\mathbf{X}}^T + \dot{\boldsymbol{\lambda}} = \mathbf{0} \rightarrow \dot{\boldsymbol{\lambda}} = -\mathbf{f}_{\mathbf{X}}^T \boldsymbol{\lambda} - \mathcal{G}_{\mathbf{X}}^T \tag{61}$$

$$\boldsymbol{\upsilon} = \mathbf{0} \rightarrow \mathcal{G}_{\mathbf{X}} = \mathbf{0}, \ \frac{d}{d\mathbf{X}} \begin{Bmatrix} \dot{\alpha} & \dot{e}_x & \dot{e}_y \end{Bmatrix}^T = \mathbf{0} \tag{62}$$

$$\boldsymbol{\lambda} = \boldsymbol{\Phi} \boldsymbol{\lambda}_f, \ \boldsymbol{\Phi} = \mathbf{I}_{4x4} + \begin{bmatrix} \mathbf{0}_{4x3} & \int_n^0 \left(\partial \dot{t} / \partial \mathbf{X} \right)^T ds \end{bmatrix} \tag{63}$$

$$H_{\boldsymbol{\upsilon}} = \mathbf{0} \rightarrow \boldsymbol{\upsilon} = -w_m^{-1} \mathbf{f}_{\boldsymbol{\upsilon}}^T \boldsymbol{\Phi} \boldsymbol{\lambda}_f \tag{64}$$

We begin with the solution of axial elements from the first approximation Eq. (47) in order to determine **f**, w_m, and **Φ**, but do not require a control history or guess for the Lagrange multipliers. For simplicity we set the controls to zero and artificially constrain the orbital elements to their initial state causing a first-order change in $\dot{t}$ as shown in Eq. (65), which gives the error in the final state. We seek a control history that propagates the system to the final state in Eq. (66), where $\boldsymbol{\Phi}^T$ maps changes in **f** to the final state because of the backward propagation in Eq. (63). The system of Eqs. (66) solves the set $\boldsymbol{\lambda}_f$ and corresponding control that targets the final state, and is numerically efficient because it only considers the four in-plane elements and is positive definite. The new control history Eq. (64) provides an estimate for the optimal trajectory, where **f** is *not* updated during the propagation in Eq. (67) so that $\mathbf{X}_f^* = \mathbf{X}_f$ exactly. The update to the path of axial elements and control gain w_m are restricted by a scaling factor ε to that the trajectory does not vary too much from iteration to iteration, dramatically improving convergence. We initially set $\varepsilon = 0.5$ then reduce to $\varepsilon = 0.3$ for cases that do not converge to a loose tolerance of 10^{-3} after about 10 iterations, and cases that tend toward e > 1 are discarded. The controls are artificially reset to zero for each iteration and recalculated from the updated values of **f**, w_m, and **Φ** from the new estimate of the optimal trajectory **X**.

$$\boldsymbol{\Delta} = \mathbf{X}_f - \mathbf{X}_0 - \int_0^n \begin{Bmatrix} 0 & 0 & 0 & \dot{t} - \partial \dot{t} / \partial \mathbf{X} \left(\mathbf{X} - \mathbf{X}_0 \right) \end{Bmatrix}^T ds \tag{65}$$

$$\boldsymbol{\Delta} = \int_0^n \boldsymbol{\Phi}^T \mathbf{f}_{\boldsymbol{\upsilon}} \boldsymbol{\upsilon} ds = \left(\int_0^n -\boldsymbol{\Phi}^T \mathbf{f}_{\boldsymbol{\upsilon}} w_m^{-1} \mathbf{f}_{\boldsymbol{\upsilon}}^T \boldsymbol{\Phi} ds \right) \boldsymbol{\lambda}_f \tag{66}$$

$$\mathbf{X}^* = \mathbf{X}_0 + \int_0^n \mathbf{f}_{\boldsymbol{\upsilon}} \mathbf{u} ds \tag{67}$$

$$\mathbf{X}_{i+1} = \mathbf{X}_i + \varepsilon \left(\mathbf{X}^* - \mathbf{X}_i \right), \ w_{m,i+1} = w_{m,i} + \varepsilon \left(w_m^* - w_{m,i} \right), \ 0 < \varepsilon \leq 1 \tag{68}$$

Once the in-plane motion has been determined optimization of the out-of-plane motion requires only one iteration. Because h_X and h_Y do not influence the dynamics, their Lagrange multipliers Eq. (69) are constant. As in Eq. (64) the optimal control is a function of the associated Lagrange multipliers, and the path of the orbital plane is ultimately determined by their solution in Eq. (71).

$$\dot{\lambda}_{h_X} = 0, \ \dot{\lambda}_{h_Y} = 0 \tag{69}$$

$$u_h = -w_m^{-1} \mathbf{h}_u \begin{Bmatrix} \lambda_{h_X} & \lambda_{h_Y} \end{Bmatrix}^T, \ \mathbf{h}_u = \begin{Bmatrix} \partial \dot{h}_X / \partial u_h & \partial \dot{h}_Y / \partial u_h \end{Bmatrix} \tag{70}$$

$$\begin{Bmatrix} 0 & h_{Y,f} \end{Bmatrix} = \begin{Bmatrix} \lambda_{h_X} & \lambda_{h_Y} \end{Bmatrix} \int_0^n -\mathbf{h}_u w_m^{-1} \mathbf{h}_u^T ds \tag{71}$$

Optimal Bounded Control

At this point the low thrust transfers are modeled accurately enough to estimate propellant over the transfer and the maximum deliverable mass, but the thruster model Eq. (55) is inaccurate for typical thrusters with constant exhaust velocity $c = gI_{sp}$. The thruster model Eq. (72) solves this issue where $Thrust/(-dm/dt) = c$ when the thrust τ_T and flow rate τ_m throttles are equal. A major cause of consternation while optimizing low-thrust transfers with constant specific impulse is accounting for the "bang-bang" control of when the thrust should be fully on or fully off. To this end a new formulation for the thrust and flow-rate throttles is developed in Eq. (73), where u_m is the governing throttle control. The thrust and flow rate throttle map from 0 to 1 as the control increases from 0 to 1 in Figure 1. This formulation employs a parameter β that is varied from 1 to 0, where the model is less accurate but robustly converges near 1, and accurately models a constant-specific-impulse thruster with bang-bang control at 0. When $\beta > 0$ in Figure 1 $\tau_T > \tau_m$ which overestimates the specific impulse at low throttle, but when $\beta = 0$ in Eq. (73) $\tau_T = \tau_m$ and the specific impulse is constant for all u_m. This approximation is particularly suited to algorithms that take advantage of fixed segment placement where adjusting segment boundaries to the exact switch times (as in Ref [8]) would disrupt the underlying structure. In addition to the throttle control, the unit vector $\boldsymbol{l}$ controls the direction of thrust so that $\mathbf{u}$ takes the form of Eq. (76).

$$\begin{aligned} Thrust &= \tau_T \, 2P_1 (AU/r)^2 / c \\ dm/dt &= -\tau_m \, 2P_1 (AU/r)^2 / c^2 \end{aligned} \tag{72}$$

$$\begin{aligned} \tau_T &= \beta u_m + (3-2\beta) u_m^2 - (2-\beta) u_m^3 \\ \tau_m &= (3-\beta) u_m^2 - (2-\beta) u_m^3 \end{aligned} \tag{73}$$

$$dm/dL = -\tau_m \, 2P_1 AU^2 \Big/ \left[c^2 \sqrt{\mu a (1 - e_X^2 - e_Y^2)} \right] \tag{74}$$

$$\dot{m} = \tau_m w_m, \; w_m = -2P_1 AU^2 \Delta L \Big/ \left[c^2 \sqrt{\mu a (1 - e_X^2 - e_Y^2)} \right] \tag{75}$$

$$\mathbf{u} = \tau_T w_T \boldsymbol{l} / m, \; w_T = \mu 2P_1 AU^2 / c \tag{76}$$

$$\boldsymbol{l} = \{ l_r \quad l_\theta \quad l_h \}^T, \; \boldsymbol{l}^T \boldsymbol{l} = 1 \tag{77}$$

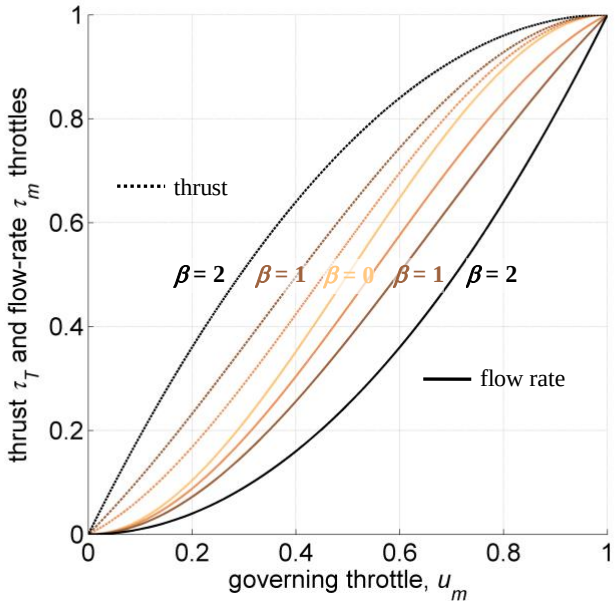

Figure 1 The thruster model approaches constant specific impulse as β approaches 0.

The objective function for this final step is to maximize the final mass for a fixed initial mass and the full state, now including mass, is considered during optimization. The final value for the mass Lagrange multiplier is -1 from the objective Eq. (78), leaving the other 6 multipliers in Eq. (78) as unknowns to target the final state. The associated Hamiltonian for this problem Eq. (81) includes a Lagrange multiplier λ_l for the thrust direction constraint but the throttle control is ostensibly left unconstrained. The Hamiltonian is rearranged by collecting the partials of H with respect to $\mathbf{u}$ in Eq. (82) to highlight the effect of $\boldsymbol{l}$ on H. By inspection, H is minimized (a necessary condition for optimality [7]) by pointing opposite $H_{\mathbf{u}}$ in Eq. (84). (An alternative approach solves for λ_l in Eq. (85).)

$$J = -mf \tag{78}$$

$$\begin{aligned} \mathbf{X} &= \left\{\alpha \quad e_X \quad e_Y \quad h_X \quad h_Y \quad t \quad m\right\}^T, \ \mathbf{f} = \dot{\mathbf{X}} \\ \boldsymbol{\lambda} &= \left\{\lambda_\alpha \quad \lambda_{e_X} \quad \lambda_{e_Y} \quad \lambda_{h_X} \quad \lambda_{h_Y} \quad \lambda_t \quad \lambda_m\right\}^T \end{aligned} \tag{79}$$

$$\boldsymbol{\lambda}_f = \left\{\lambda_\alpha \quad \lambda_{e_X} \quad \lambda_{e_Y} \quad \lambda_{h_X} \quad \lambda_{h_Y} \quad \lambda_t\right\}^T\Big|_{s=n} \tag{80}$$

$$H = \boldsymbol{\lambda}^T\mathbf{f} + \lambda_l\left(\boldsymbol{l}^T\boldsymbol{l} - 1\right) \tag{81}$$

$$H = \left(H_r l_r + H_\theta l_\theta + H_h l_h\right)\tau_T w_T / m + \lambda_m \tau_m w_m + \lambda_t \dot{t} + \lambda_l\left(\boldsymbol{l}^T\boldsymbol{l} - 1\right) \tag{82}$$

$$\begin{aligned} H_r &= \partial H/\partial u_r = \lambda_\alpha\, \partial\dot{\alpha}/\partial u_r + \lambda_{e_X}\, \partial\dot{e}_X/\partial u_r + \lambda_{e_Y}\, \partial\dot{e}_Y/\partial u_r \\ H_\theta &= \partial H/\partial u_\theta = \lambda_\alpha\, \partial\dot{\alpha}/\partial u_\theta + \lambda_{e_X}\, \partial\dot{e}_X/\partial u_\theta + \lambda_{e_Y}\, \partial\dot{e}_Y/\partial u_\theta \\ H_h &= \partial H/\partial u_h = \lambda_{h_X}\, \partial\dot{h}_X/\partial u_h + \lambda_{h_Y}\, \partial\dot{h}_Y/\partial u_h \end{aligned} \tag{83}$$

$$\mathbf{l} = -\{H_r \quad H_\theta \quad H_h\}^T \Big/ \sqrt{H_r^2 + H_\theta^2 + H_h^2} \tag{84}$$

$$H_{\mathbf{l}} = \{H_r \quad H_\theta \quad H_h\} + 2\lambda_1 \mathbf{l}^T = 0 \rightarrow \lambda_1 = \sqrt{H_r^2 + H_\theta^2 + H_h^2}\,/2 \tag{85}$$

After applying Eq. (84) the optimal throttle level causes the partial in Eq. (86) to vanish and solving Eq. (87), where σ acts as a switching function. The optimal value for the throttle Eq. (89) always remains between zero and one as demonstrated in Figure 2. The parameter β implicitly smoothes the control and walks the throttle towards a bang-bang structure. However, unlike an explicit smoothing function the value of u_m in Eq. (89) is the exact optimal solution for a given value of β.

$$\partial H/\partial u_m = -\left(w_T \sqrt{H_r^2 + H_\theta^2 + H_h^2}\,/m\right)\partial\tau_T/\partial u_m + \left(\lambda_m w_m\right)\partial\tau_m/\partial u_m = 0 \tag{86}$$

$$\beta\sigma - 2\left[(3-2\beta)(1-\sigma)+\beta\right]u_m + 3(2-\beta)(1-\sigma)u_m^2 = 0 \tag{87}$$

$$\sigma = w_T \sqrt{H_r^2 + H_\theta^2 + H_h^2}\,\Big/\left(m\lambda_m w_m\right) \tag{88}$$

$$u_m = \begin{cases} k_0 \Big/ \left(\sqrt{k_1^2 - k_0} - k_1\right) & \sigma < 1 \\ 1/2 & \sigma = 1 \\ \sqrt{k_1^2 - k_0} - k_1 & \sigma > 1 \end{cases} \tag{89}$$

$$k_0 = \beta\sigma/k_2,\ k_1 = -\left[(3-2\beta)(1-\sigma)+\beta\right]/k_2,\ k_2 = 3(2-\beta)(1-\sigma)$$

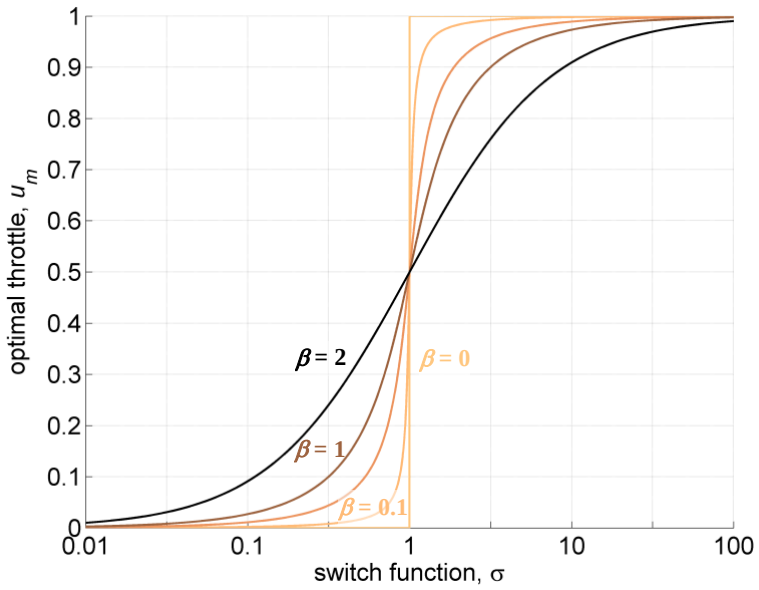

Figure 2 The throttle control optimally remains below the maximum level and adopts an on/off structure as β approaches 0.

The optimization process begins with the solution for the axial elements, control **u**, and **λ**, from the suboptimal refinement step. An initial guess for the mass is available by propagating Eq. (57), and the

initial flow-rate is approximated by equating Eq. (57) and Eq. (75) in Eq. (90). The Lagrange multipliers are propagated backwards from their final values and separated into a term that depends on the final mass Eq. (91) and a term from the state transition matrix Eq. (92). This propagation is simplified somewhat by noting that $\partial\mathbf{f}/\partial\{h_X \quad h_Y \quad t\} = 0$. The new history of $\boldsymbol{\lambda}$ produces an updated control $\mathbf{u}$ in Eq. (76) via Eqs. (84) and (89). This new control then creates a departure from the original path for the in-plane parameters α, e_X, e_Y in Eq. (94), which in turn changes the flight time in Eq. (95). The error in the final state is collected in Eq. (97), and the sensitivities are mapped back to $\boldsymbol{\lambda}_f$ in Eq (98) leading to an update in the estimate of $\boldsymbol{\lambda}$ in Eq. (99). Instead of performing a full iteration and recalculating Eqs. (48), the error $\boldsymbol{\Delta}$ is first driven down by iterating on Eqs. (93)–(99) while holding m, w_m, $\mathbf{f_u}$, and $\boldsymbol{\Phi}$ fixed, so that the optimization of the control occurs without varying the state sensitivities. After a few sub-iterations (3 tends to work well) the new controls $\mathbf{u}$ and τ_m update the previous guess in step restricted by ε (similar to Eq. (68)). A new estimate for the optimal trajectory is produced by propagating the variational Eqs. (48) and (75) while holding $\mathbf{u}$ and τ_m fixed, so that the path update occurs without varying the controls. This decoupling of the state and control dynamics results in a marked improvement of the region of convergence.

$$\tau_m = \mathbf{u}^T\mathbf{u}\left[mc\mu/\left(2P_1AU^2\right)\right]^2 \tag{90}$$

$$\dot{\boldsymbol{\lambda}}^* = -\mathbf{f}_\mathbf{X}^T\boldsymbol{\lambda}^*, \ \boldsymbol{\lambda}_f^* = \{\mathbf{0}_{1x6} \quad -1\} \tag{91}$$

$$\dot{\boldsymbol{\Phi}} = -\mathbf{f}_\mathbf{X}^T\boldsymbol{\Phi}, \boldsymbol{\Phi}_f = \begin{bmatrix}\mathbf{I}_{6x6}\\ \mathbf{0}_{1x6}\end{bmatrix} \tag{92}$$

$$\boldsymbol{\lambda} = \boldsymbol{\lambda}^* + \boldsymbol{\Phi}\boldsymbol{\lambda}_f \tag{93}$$

$$\mathbf{E}(s) = \int\{\dot{\alpha} \quad \dot{e}_X \quad \dot{e}_Y\}\,ds - \{\alpha-\alpha_0 \quad e_X - e_{X,0} \quad e_Y - e_{Y,0}\} \tag{94}$$

$$t^* = \int_0^n\left(\dot{t} + \partial\dot{t}/\partial\{\alpha \quad e_X \quad e_Y\}\mathbf{E}^T\right)ds - t_f \tag{95}$$

$$\mathbf{H} = \int_0^n\{\dot{h}_X \quad \dot{h}_Y\}ds - \{0 \quad h_{Y,f}\} \tag{96}$$

$$\boldsymbol{\Delta} = \{\mathbf{E}_f \quad \mathbf{H} \quad t^*\}^T \tag{97}$$

$$\partial\boldsymbol{\Delta}/\partial\boldsymbol{\lambda}_f = \int_0^n\begin{bmatrix}\mathbf{I}_{5x7}\\ \boldsymbol{\Phi}(\mathbf{X},t)^T\end{bmatrix}\mathbf{f}_\mathbf{u}\left(\partial\mathbf{u}/\partial\boldsymbol{\lambda}\right)\boldsymbol{\Phi}ds \tag{98}$$

$$\boldsymbol{\Delta} + \left(\partial\boldsymbol{\Delta}/\partial\boldsymbol{\lambda}_f\right)\Delta\boldsymbol{\lambda}_f = \mathbf{0} \tag{99}$$

$$\mathbf{u}_{i+1} = \mathbf{u}_i + \varepsilon\left(\mathbf{u}-\mathbf{u}_i\right), \tau_{m,i+1} = \tau_{m,i} + \varepsilon\left(\tau_m - \tau_{m,i}\right), \ 0 < \varepsilon \le 1 \tag{100}$$

RESULTS

We first consider individual transfers to Mars to investigate the behavior of the optimization sequence. In Figure 3 the path of the first approximation determines the number of revolutions around the sun and locks in the segment spacing with respect to true longitude, implicitly solving the phase problem. The linear path through eccentricity space is rather crude, but the suboptimal refinement results in a nearly optimal path of the orbital elements for the transfer in Figure 4. However, the resulting thrust profile is clearly infeasible in Figure 5, where subsequent iteration drives the solution towards feasibility with control that is optimally bounded. The algorithm is applied to a global search of transfers to Mars in Figure 6, where trajectories are generated in 5-day increments and contain 88 segments. For this problem the maximum initial mass is 30 tons (e.g. to deliver cargo for a human mission) with a jet power of 50 kW at 1 AU, and 2500 s specific impulse. Subsequent refinement produces a similar plot in Figure 7, where the control bounds and optimality conditions have been taken into account. This plot is an analogue to the "bacon plots" (i.e. SEP versions of the "pork-chop" plot) recently developed for Mars mission formulation [9]. Rendezvous with comet 63P/Wild 1 poses a more difficult problem in Figure 8. This comet has an eccentricity of 0.65, a semi-major axis of 5.6 AU, and an inclination of nearly 20 degrees. For this example the maximum initial mass is 1 ton (e.g. to deliver a robotic orbiter) with a jet power of 10 kW at 1 AU, and 2500 s specific impulse. As with the Mars example the solution with bounded controls displays the same structure as the suboptimal refinement result, with a moderate decrement in performance. A high-level assessment and comparison of the algorithm is summarized in Table 2, where the capability to run extensive trade studies with same-day turnaround of results is demonstrated.

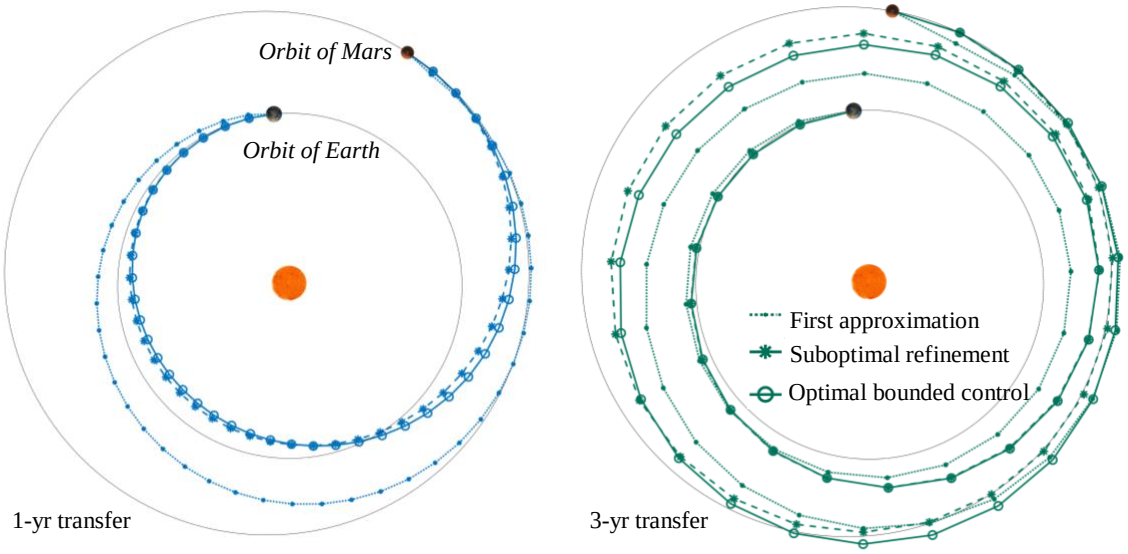

Figure 3 The number of revolutions in the first approximation shapes the optimized solution.

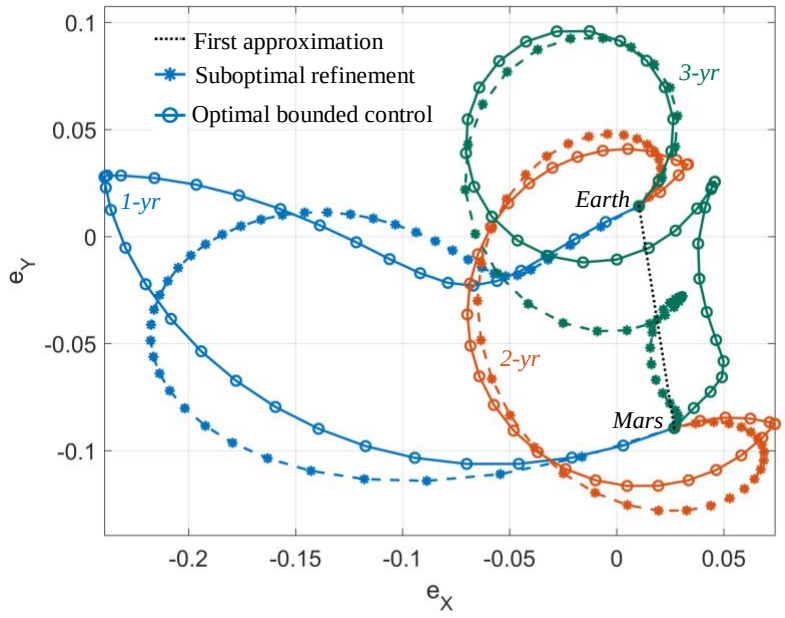

Figure 4 The suboptimal approximation closely the tracks eccentricity vector of optimal solution.

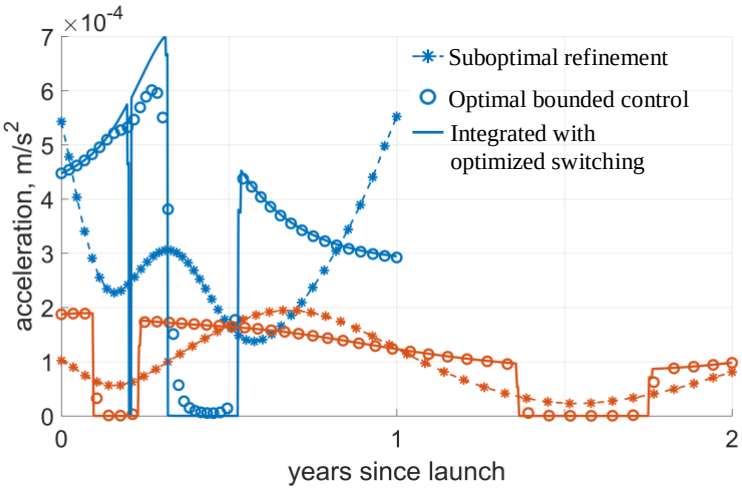

Figure 5 The bounded control matches the switch times of a fully optimized transfer.

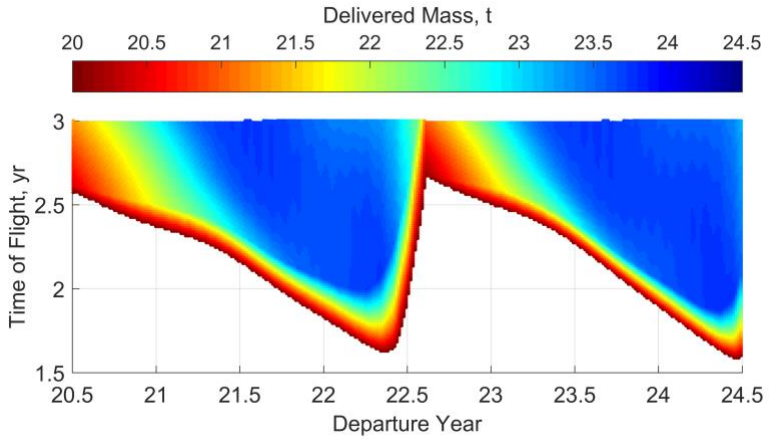

Figure 6 Trade space of transfers to Mars from suboptimal refinement step.

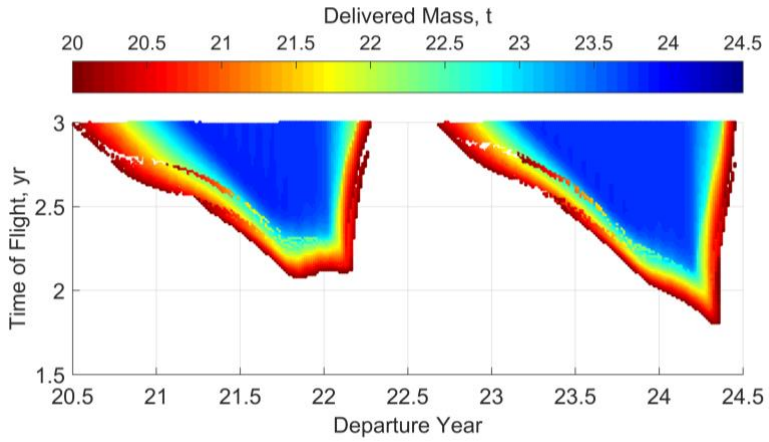

Figure 7 Optimized trade space of transfers to Mars.

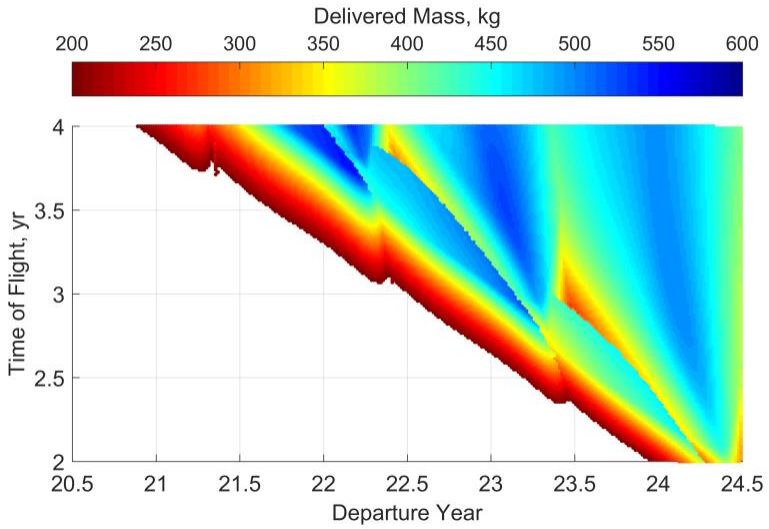

Figure 8 Trade space of transfers to 63P/Wild 1 from suboptimal refinement step.

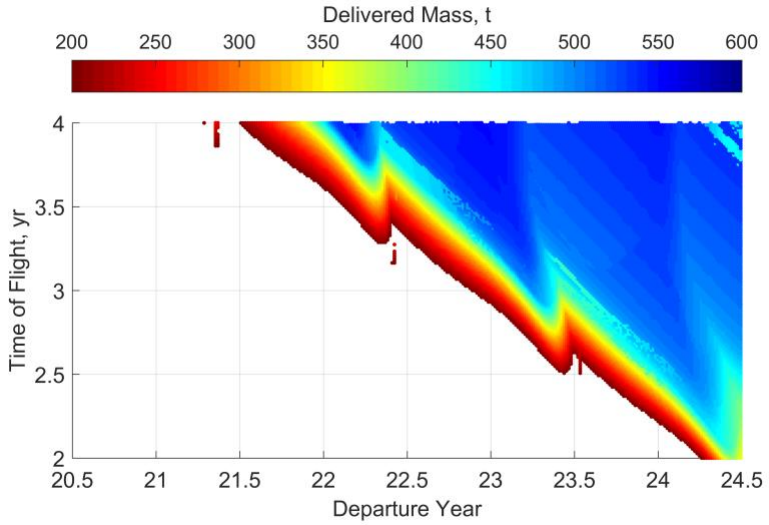

Figure 9 Optimized trade space of transfers to 63P/Wild 1.

Table 2. Summary of accuracy and run time of different approaches.

Target	*Mars*		*Wild 1*	
Solution phase	Average error in final mass	Approx. CPU time per 100,000 cases	Average error in final mass	Approx. CPU time per 100,000 cases
First approximation	10%	10 seconds	15%	10 seconds
Suboptimal refinement	7%	3 minutes	15%	3 minutes
Optimal bounded control	0.5%	1 hour	10%	2 hour
MALTO [10] (for comparison)	0.1%	½ week	0.5%	1 week
Integrated with optimized switching	—	2 weeks	—	1 month

CONCLUSION

A judicious choice of inertial coordinate frame and axial elements decouples the in-plane and out-of-plane dynamics and allows for a semi-analytical initial guess of low-thrust interplanetary transfers. This first approximation permits a very rapid characterization of the trajectory trade space for suboptimal unbounded controls. This suboptimal refinement in turn initializes optimization of thrust controls that are optimally bounded for an accurate representation of the trajectory trade-space. The region of convergence of the optimal control problem increases by alternating between solving for the optimal controls on a fixed path and propagation of a new path with fixed controls, as opposed to propagating the state and co-state dynamics simultaneously. The convergence properties are improved further by a novel control formulation where the throttle optimally remains between minimum and maximum bounds as a bang-bang thrusting structure develops. The run time to develop a full trajectory trade space is reduced by orders of magnitude, permitting real-time formulation of low-thrust interplanetary missions.

ACKNOWLEDGMENTS

This research was carried out at the Jet Propulsion Laboratory, California Institute of Technology, under a contract with the National Aeronautics and Space Administration.

REFERENCES

[1] Cefola, P. J., "Equinoctial Orbit Elements—Application to Artificial Satellite Orbits," Paper AIAA 72-937, AIAA/AAS Astrodynamics Conference, Palo Alto, CA, September 11–12, 1972.

[2] Hintz, G. R., "Survey of Orbit Element Sets," *Journal of Guidance, Control, and Dynamics*, Vol 31, May–June 2008, pp. 785–790.

[3] Edelbaum, T. N., "Optimum Low-Thrust Rendezvous and Station Keeping," *Journal of Spacecraft and Rockets*, Vol. 2, July 1964, pp. 1196–1201.

[4] Edelbaum, T. N., "Optimum Power-Limited Orbit Transfer in Strong Gravity Fields," *AIAA Journal*, Vol. 3, May 1965, pp. 921–925.

[5] Colombo, C., Vasile, M., Radice, G., "Semi-Analytical Solution for the Optimal Low-Thrust Deflection of Near-Earth Objects," *Journal of Guidance Control, and Dynamics*, Vol. 32, May–June 2009, pp. 796–809.

[6] Zuiani, F., Vasile, M., Palmas, A., Avanzini, G, "Direct Transcription of Low-Thrust Trajectories with Finite Trajectory Elements," *Acta Astronautica*, Vol. 72, 2012, pp. 108–120.

[7] Bryson, A. E. and Ho, Y.-C., *Applied Optimal Control*, Blaisdell Publishing, Waltham, MA, 1969.

[8] Russell, R. P., "Primer Vector Theory Applied to Global Low-Thrust Trade Studies," *Journal of Guidance, Control, and Dynamics*, Vol. 30, March–April, 2007, pp. 460–472.
[9] Woolley, R. C., Baker, J. D., Landau, D. F., Post, K. E., "Low-Thrust Trajectory Maps (Bacon Plots) to Support a Human Mars Surface Expedition," Paper AAS 17-652, AAS/AIAA Astrodynamics Specialist Conference, Stevenson, WA, August 20–24, 2017.
[10] Sims, J. A. et al., "Implementation of a Low-Thrust Trajectory Optimization Algorithm for Preliminary Design," AIAA/AAS Astrodynamics Specialist Conference, Paper AIAA 2006-6746, August 2006.